Available online at www.sciencedirect.com
ScienceDirect
Journal of Molecular Catalysis A: Chemical 284 (2008) 8–15
JOURNAL OF MOLECULAR CATALYSIS A: CHEMICAL
www.elsevier.com/locate/molcata

Paired interacting orbitals (PIO) study of molybdena-alumina system active in alkene metathesis

Jarosław Handzlik [a,*], Akinobu Shiga [b], Joanna Kondziołka [a]

[a] *Institute of Organic Chemistry and Technology, Cracow University of Technology, ul. Warszawska 24, PL 31-155 Kraków, Poland*
[b] *LUMMOX Research Laboratory, Takezono 2-18-4-302, Tsukuba 305-0032, Japan*

Received 6 October 2007; received in revised form 18 December 2007; accepted 28 December 2007
Available online 4 January 2008

Abstract

The first step of the catalytic cycle of ethene metathesis on molybdena-alumina catalyst, i.e., ethene addition to surface Mo methylidene centres, is investigated by using the paired interacting orbitals (PIO) analysis based on the extended Hückel method. It is shown that the PIO theory is an adequate approach for both qualitative and quantitative description of the process. The total overlap population between the Mo methylidene part and the C_2H_4 fragment of the Mo ethene–methylidene complex decreases with a decrease of the reactivity of the Mo methylidene centre towards ethene. Therefore, the total overlap population is expected to be a useful reactivity index for the molybdenum-based olefin metathesis catalysts.

Keywords: Molybdenum; Alumina; Catalyst; Metathesis; Paired interacting orbitals

1. Introduction

Supported Mo systems are known as efficient catalysts for olefin metathesis [1–10]. Molybdena-alumina catalyst is involved in the large-scale Shell Higher Olefins Process (SHOP), where linear higher olefins are produced from ethene. The process consists of several steps, one of them being cross-metathesis of linear alkenes [1–3].

According to the commonly accepted carbene mechanism [1,11], Mo alkylidene and molybdacyclobutane species are present on the catalyst surface. They are usually generated by treatment of the catalyst precursor with alkene [1,4–9] or cycloalkane [1,10]. As the concentration of the active sites in the molybdena-alumina system is very low [12], their detailed structure has not been experimentally determined, so far. On the other hand, theoretical DFT investigations of metathesis active Mo sites on alumina were performed, using cluster models [13,14]. It was concluded that the reactivity of the Mo alkylidene sites towards alkene depends on their geometrical and electronic structure parameters, both influenced by the location of the Mo centre on the alumina surface.

The paired interacting orbitals (PIO) theory [15,16] was successfully applied in investigations of various catalytic processes involving solid catalysts [17–19]. In this work, we study qualitatively and quantitatively the interaction between ethene and Mo methylidene centres on alumina, using the PIO analysis. Addition of alkene to Mo alkylidene surface complex, leading to the molybdacyclobutane intermediate, is the first step of the metathesis reaction. The main purpose of the present work is testing whether the PIO analysis based on extended Hückel molecular orbitals is an adequate tool for description of the initial stage of the metathesis process and for the prediction of the reactivity of the surface Mo alkylidene species. Such calculations are not time consuming, in contrast to more advanced quantum chemistry methods. This is an advantage of the proposed approach, especially when relatively large systems are investigated.

2. Computational details

2.1. Models

Cluster models of the Mo methylidene sites on γ-alumina (**1**–**6**, Fig. 1), the corresponding ethene complexes (**2et**–**6et**) and the transition states leading to the molybdacyclobutane intermediates (**1ts**–**6ts**) were described previously [13,14]. In the case

* Corresponding author. Tel.: +48 12 6283072; fax: +48 12 6282037.
E-mail address: jhandz@pk.edu.pl (J. Handzlik).

1381-1169/$ – see front matter © 2008 Elsevier B.V. All rights reserved.
doi:10.1016/j.molcata.2007.12.028

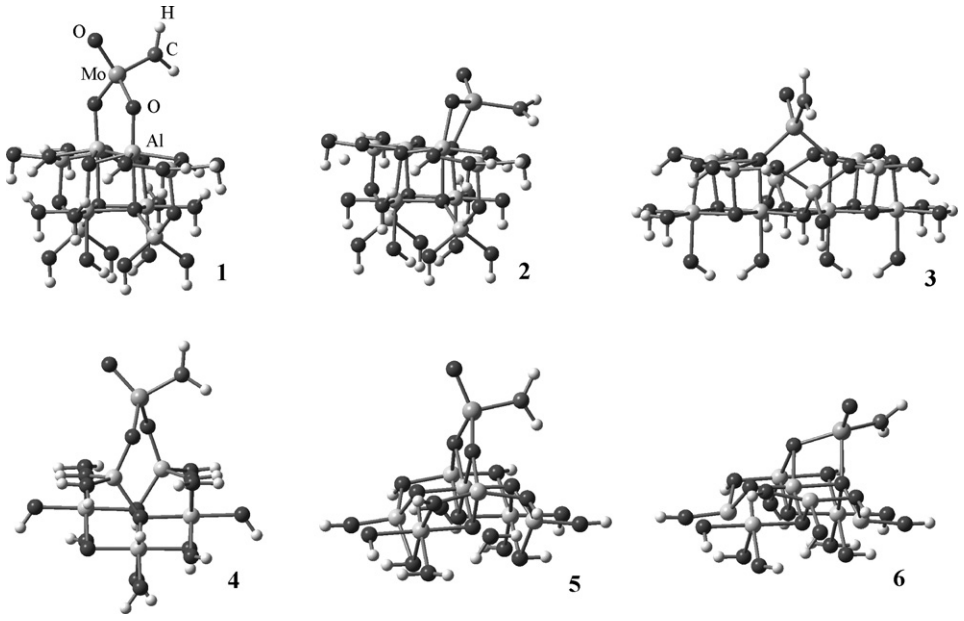

Fig. 1. Cluster models of the Mo methylidene centres on γ-alumina.

of the structures **1**–**3**, the Mo centres are placed on the (1 0 0) surface of γ-alumina, while the models **4**–**6** concern the Mo sites located on the (1 1 0) alumina face. The geometries of the Mo species and the first layer of the alumina parts of the models were optimised using density functional theory. The exception is the ethene complex **1et**, having an arbitrarily assumed geometry based on the optimised geometries of the structures **1** and **4et**. This is because the ethene complex **1et** was not localised as a minimum on the potential energy surface (PES) [13].

Additionally, another series of ethene complexes models (**1et′**–**6et′**) is proposed in the present work. In Fig. 2, the example structure **1et′** is shown. In these models, the geometry of the Mo site is obtained somewhat arbitrarily, as an "average" geometry of the ethene complexes **2et**–**6et**. The geometrical details are given in Table 1. The Mo-C^1 and C^2–C^3 distances for the structures **1et′**–**6et′** are taken from the corresponding reactants, i.e., from the Mo methylidene centres and ethene.

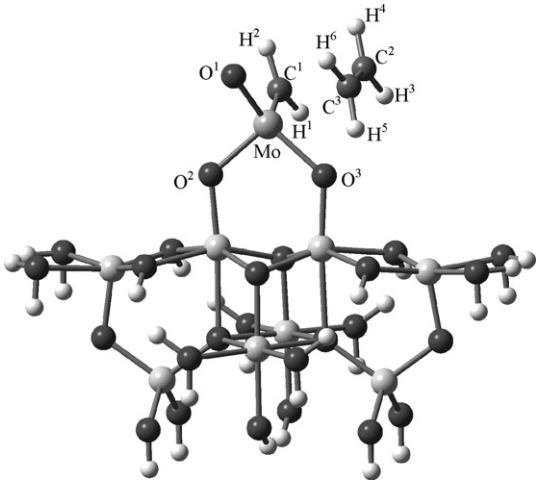

Fig. 2. The structure of the Mo ethene-methylidene complex **1et′**.

The main purpose of using approximate geometry of the ethene complexes (**1et′**–**6et′**) is obtaining reasonable approximates of their reactivity without the time-consuming geometry optimization on high level of theory. Such an approach is especially useful for large catalytic systems.

The atomic labels in Fig. 2 refer to all ethene complexes and transition states considered in this work.

2.2. DFT calculations

Geometry optimisation of the structures studied was performed using the Gaussian 03 program [20] and the B3LYP functional [21,22]. The Hay–Wadt effective core potential [23] plus double zeta basis set was applied for molybdenum. To describe C, H, O and Al atoms, the Dunning–Huzinaga full double zeta basis set (D95) [24] was employed. Single point energy calculations for the optimised structures were done using the B3LYP functional with the D95(d,p) basis set for C, O, Al and H, combined with the LANL2DZ basis set for Mo. Other details are given elsewhere [13,14]. The presented relative energies do not include the zero point energy (ZPE) corrections.

2.3. PIO calculations

Paired interacting orbitals (PIO) calculation, proposed by Fujimoto et al. [15,16], is a method for unequivocally determining the orbitals which should play dominant roles in chemical

Table 1
The geometrical parameters of the ethene complexes **1et′**–**6et′**

Mo–C^3	2.60 Å
C^1–C^2	2.84 Å
C^1–Mo–C^3	102.5°
Mo–C^3–C^2	80°
C^1–Mo–C^3–C^2	±10°

Table 2
Extended Hückel parameters

Orbital	H_{ii} (eV)	ζ_1	ζ_2
H 1s	−13.60	1.300	–
C 2s	−21.40	1.625	–
C 2p	−11.40	1.625	–
O 2s	−32.30	2.275	–
O 2p	−14.80	2.275	–
Al 3s	−12.30	1.167	–
Al 3p	−6.50	1.167	–
Mo 5s	−8.77	1.960	–
Mo 5p	−5.60	1.900	–
Mo 4d	−11.06	4.540 (0.5899[a])	1.900 (0.5899[a])

[a] Contraction coefficients.

interactions between two systems, [A] and [B], which construct a combined system [C]. Here, [C] is the ethene complex or the transition state, while [A] is the Mo methylidene fragment and [B] is the C_2H_4 fragment. The geometries of [A] and [B] are the same as those in the complex [C] ([A-B]≡[C]). The extended Hückel MOs of [A], [B] and [C] are calculated. The extended Hückel parameters are given in Table 2. PIOs are obtained by applying the procedure that was proposed by Fujimoto et al. [15,16]. It is summarized as follows:

1. We expand the MOs of the complex in terms of the MOs of two fragment species, to determine the expansion coefficients $c_{i,f}$, $c_{m+j,f}$ and $d_{k,f}$, $d_{n+l,f}$:

$$\Phi_f = \sum_{i=1}^{m} c_{i,f}\phi_i + \sum_{j=1}^{M-m} c_{m+j,f}\phi_{m+j} + \sum_{k=1}^{n} d_{k,f}\psi_k + \sum_{l=1}^{N-n} d_{n+l,f}\psi_{n+l} \quad (1)$$

where Φ are the MOs of the complex [C], ϕ and ψ are the MOs of the fragment [A] and [B], respectively, m and n indicate the number of the occupied MOs of A and B, respectively, and M and N are the total numbers of the MOs of A and B, respectively.

2. We construct an interaction matrix **P** which represents the interaction between the MOs of the fragment [A] and the MOs of the fragment [B]:

$$\mathbf{P} = \begin{pmatrix} P_{i,k} & P_{i,n+l} \\ P_{m+j,k} & P_{m+j,n+l} \end{pmatrix} \quad (2)$$

where:

$$P_{i,k} = \sum_{f=1}^{m+n} n_f c_{i,f} d_{k,f}$$

$$P_{i,n+l} = \sum_{f=1}^{m+n} n_f c_{i,f} d_{n+l,f}$$

$$P_{m+j,k} = \sum_{f=1}^{m+n} n_f c_{m+j,f} d_{k,f}$$

$$P_{m+j,n+l} = \sum_{f=1}^{m+n} n_f c_{m+j,f} d_{n+l,f}$$

$i = 1, \ldots, m$

$j = 1, \ldots, M-m$

$k = 1, \ldots, n$

$l = 1, \ldots, N-n$

n_f-the number of electrons in orbital f.

3. We get transformation matrix $\mathbf{U^A}$ (for A) and $\mathbf{U^B}$ (for B) by:

$$\mathbf{P^\dagger P U^A} = \mathbf{U^A}\Gamma \quad (3)$$

$$U^B_{s,v} = (\gamma_v)^{-\frac{1}{2}} \sum_{r}^{N} P_{r,s} U^A_{r,v} \quad v = 1, \ldots, N \quad (4)$$

4. Finally, we obtain the PIOs by Eqs. (5) and (6).

$$\phi'_v = \sum_{r}^{N} U^{\mathrm{A}}_{r,v} \phi_r \quad (\text{for A}) \quad (5)$$

$$\psi'_v = \sum_{s}^{N} U^{\mathrm{B}}_{s,v} \psi_s \quad (\text{for B}) \quad (6)$$

The $N \times M$ orbital interactions in the complex C can thus be reduced to the interactions of N PIOs, N indicating the smaller of the numbers of the MOs of the two fragments, A and B.

PIO calculations have been carried out on the *LUMMOX*™ system [25,26].

3. Results and discussion

3.1. PIO analysis of the ethene complexes

The first step of ethene metathesis is ethene addition to Mo alkylidene centre. In most cases, ethene complexes were localised as minima on the PES at early stage of the reaction [13,14]. In Table 3, the eigenvalues of the first seven PIOs for the ethene complexes **1et**–**6et** are presented. It can be seen that

Table 3
The eigenvalues of the PIOs of the ethene complexes

	PIO-1	PIO-2	PIO-3	PIO-4	PIO-5	PIO-6	PIO-7
1et	0.191	0.077	0.024	0.009	0.004	0.003	0.002
2et	0.241	0.136	0.022	0.012	0.006	0.003	0.003
3et	0.203	0.092	0.032	0.016	0.007	0.005	0.004
4et	0.192	0.079	0.017	0.008	0.004	0.003	0.002
5et	0.251	0.145	0.025	0.015	0.007	0.005	0.003
6et	0.268	0.195	0.021	0.016	0.008	0.006	0.003

Table 4
The occupation numbers of the PIOs of the ethene complexes

	PIO-1			PIO-2			PIO-3		
	Catalyst	C_2H_4	Total	Catalyst	C_2H_4	Total	Catalyst	C_2H_4	Total
1et	0.59	1.78	2.37	1.78	0.57	2.35	1.61	1.90	3.51
2et	0.45	1.70	2.15	1.81	0.51	2.32	1.58	1.95	3.53
3et	0.56	1.74	2.30	1.69	0.63	2.32	1.63	1.95	3.58
4et	0.50	1.77	2.27	1.79	0.56	2.35	1.65	1.86	3.51
5et	0.53	1.68	2.21	1.75	0.55	2.30	1.61	1.92	3.53
6et	0.57	1.61	2.18	1.66	0.57	2.23	1.43	1.94	3.37

the PIO-1 and PIO-2 have a dominant contribution to the interaction between the catalyst and ethene, however the principal interaction is represented by the PIO-1. The contribution of the PIO-3 is much smaller but not meaningless, while the remaining PIOs do not seem to be important.

The presentation of the PIO-1 and PIO-2 in terms of linear combinations of the canonical MOs indicates that the catalyst part of the PIO-1 is composed mainly of the LUMO (the Lowest Unoccupied Molecular Orbital), while the ethene part of the PIO-1 is almost the pure HOMO (the Highest Occupied Molecular Orbital). On the other hand, the PIO-2 of ethene is composed mainly of the LUMO, whereas the dominant component of the PIO-2 of the Mo methylidene centre is the HOMO. Below, the example LCMO representations of the PIO-1 (ϕ'_1, ψ'_1) and PIO-2 (ϕ'_2, ψ'_2) of the alkene complex **5et** are presented. The subscripts at the PIO components indicate the numbers of the canonical MOs.

The catalyst part:

$$\phi'_1 = 0.13\phi_{22} - 0.11\phi_{87} + 0.17\phi_{88}(\text{HOMO}) + 0.73\phi_{89}(\text{LUMO}) - 0.47\phi_{91} - 0.21\phi_{92} + 0.32\phi_{93} + \cdots$$

$$\phi'_2 = -0.11\phi_{22} + 0.24\phi_{87} - 0.93\phi_{88}(\text{HOMO}) + 0.14\phi_{89}(\text{LUMO}) - 0.10\phi_{91} + \cdots$$

The C_2H_4 part:

$$\psi'_1 = -0.14\psi_5 - 0.96\psi_6(\text{HOMO}) + 0.22\psi_7(\text{LUMO}) + \cdots$$

$$\psi'_2 = -0.18\psi_1 - 0.38\psi_2 - 0.10\psi_5 - 0.22\psi_6(\text{HOMO}) - 0.86\psi_7(\text{LUMO}) + 0.11\psi_{12} + \cdots$$

The HOMO of the Mo methylidene complex is composed largely of the $2p_z$ orbital of C^1 and the $4d_{xz}$ orbital of Mo, while the LUMO is a mixture of mainly the Mo $4d_{z2}$ and $4d_{xz}$ orbitals (the Mo=C bond is parallel to the x axis and the methylidene group defines the xy plane). The HOMO and LUMO of ethene are, of course, π and π^* orbitals, respectively, composed predominantly of the $2p_z$ orbitals. Therefore, the mentioned atomic orbitals are the main components of the PIO-1 and PIO-2. For example, the LCAO representations of the PIO-1 and PIO-2 of the ethene complex **5et** are given below.

The catalyst part:

$$\phi'_1 = -0.21\text{Mo5s} - 0.28\text{Mo5p}_z - 0.83\text{Mo4d}_{z2} + 0.32\text{Mo4d}_{xz} + 0.14\text{O}^1\text{2p}_z + 0.15\text{O}^2\text{2p}_x + 0.17\text{O}^2\text{2p}_y + 0.13\text{O}^2\text{2p}_z + 0.18\text{O}^3\text{2p}_z + \cdots$$

$$\phi'_2 = -0.10\text{Mo5s} - 0.16\text{Mo4p}_z + 0.14\text{Mo4d}_{z2} - 0.47\text{Mo4d}_{xz} - 0.10\text{C}^1\text{2s} - 0.10C^1\text{2p}_x - 0.70\text{C}^1\text{2p}_z + 0.10\text{O}^1\text{2p}_z + \cdots$$

The C_2H_4 part:

$$\psi'_1 = 0.43\text{C}^2\text{2p}_z + 0.79\text{C}^3\text{2p}_z + \cdots$$

$$\psi'_2 = 0.84\text{C}^2\text{2p}_z + 0.14\text{C}^3\text{2p}_x - 0.55\text{C}^3\text{2p}_z + 0.23\text{H}^3\text{1s} + 0.24\text{H}^4\text{1s} - 0.10\text{H}^5\text{1s} + \cdots$$

In Table 4, the occupation numbers of electrons for the PIO-1, PIO-2 and PIO-3 are listed. The C_2H_4 part of the PIO-1 is more occupied than the Mo methylidene part, on the contrary to the PIO-2. Thus, the PIO-1 represents electron delocalisation from the occupied π orbital of ethene to the unoccupied orbitals of the Mo methylidene centre, mainly d_{z2}, while the PIO-2 shows back-donation from the occupied space of the Mo site, contributed mainly from the C^1 $2p_z$ and Mo $4d_{xz}$ orbitals, to the ethene π^* orbital.

In Table 5, the overlap populations (OP) of the PIO-1, PIO-2 and PIO-3 are listed. In Fig. 3, example contour maps of these orbitals for the alkene complex **5et** are plotted. One can notice relatively high positive values of the OP of the PIO-1 and the in-

Table 5
The overlap populations of the PIOs of the ethene complexes

	PIO-1	PIO-2	PIO-3
1et	0.132	0.021	−0.044
2et	0.245	0.044	−0.051
3et	0.150	0.025	−0.003
4et	0.153	0.020	−0.037
5et	0.228	0.048	−0.057
6et	0.267	0.076	−0.048

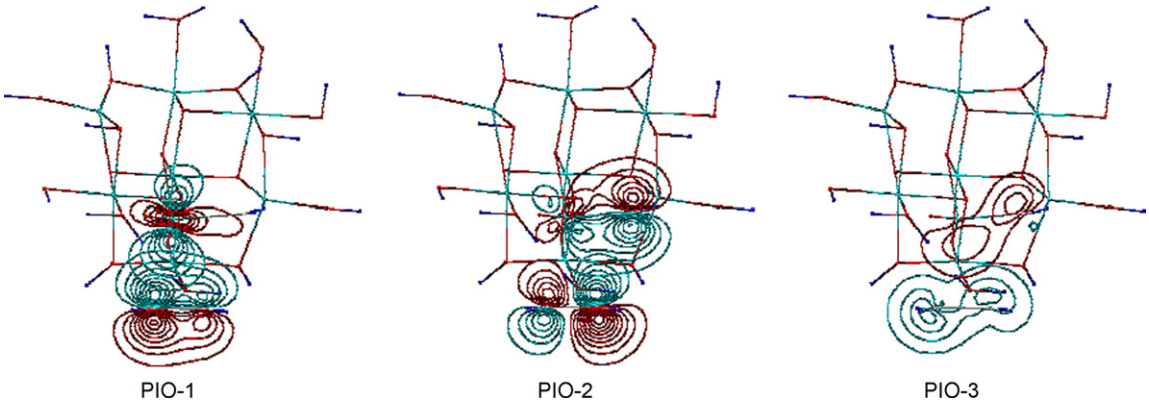

Fig. 3. Countur maps of the PIO-1, PIO-2 and PIO-3 of the ethene complex **5et**.

phase overlap. On the other hand, the positive values of the OP of the PIO-2 are much lower and the overlap can be hardly seen. As the PIO-3 is concerned, the OP value is negative (Table 5), indicating the repulsive interaction and no overlap (Fig. 3). In this case, both orbital parts of the catalyst and ethene are occupied (Table 4), which explains the antibonding character of the PIO-3.

The obtained results indicate that a nucleophilic attack with a dominant interaction between the HOMO of ethene and the unoccupied orbitals of the Mo methylidene site takes place at the early stage of the reaction. This is consistent with other reported studies [27] and with the previous DFT investigations of the molybdena-alumina metathesis catalysts [13,14]. As the result of this donation, a σ bond is formed between the molybdenum and C_2H_4 (Fig. 3). The back-donation is less significant (Table 5, Fig. 3) and the C1–C2 bond is not formed yet.

3.2. PIO analysis of the transition states

The structures **1ts**–**6ts** are the saddle points localised on the PES by using DFT [13,14]. They connect the ethene complexes and the corresponding molybdacyclobutane intermediates. On the basis of the eigenvalues of the PIOs for the transition states (Table 6), it can be stated that the PIO-1 and PIO-2 represent the principal interactions.

The presentation of the PIO-1 and PIO-2 in terms of linear combinations of the canonical MOs shows significant contributions of both HOMO and LUMO in PIO-1 and PIO-2. In the case of the C_2H_4 part, the LUMO contribution to the PIO-1 is dominant, while the HOMO content is largest in the PIO-2. The example LCMO representations of the PIO-1 and PIO-2 of **5ts** are presented below.

Table 6
Eigenvalues of the PIOs of the transition states

	PIO-1	PIO-2	PIO-3	PIO-4	PIO-5	PIO-6	PIO-7
1ts	0.447	0.336	0.044	0.028	0.023	0.014	0.008
2ts	0.529	0.399	0.066	0.035	0.029	0.015	0.012
3ts	0.497	0.368	0.056	0.039	0.027	0.020	0.013
4ts	0.436	0.336	0.043	0.025	0.023	0.014	0.008
5ts	0.473	0.362	0.050	0.031	0.026	0.014	0.009
6ts	0.493	0.362	0.055	0.029	0.024	0.011	0.009

The catalyst part:

$$\phi_1' = 0.19\phi_{22} - 0.26\phi_{87} + 0.75\phi_{88}(\text{HOMO}) - 0.49\phi_{89}(\text{LUMO}) - 0.24\phi_{91} - 0.11\phi_{93} + \cdots$$

$$\phi_2' = 0.14\phi_{87} - 0.57\phi_{88}(\text{HOMO}) - 0.69\phi_{89}(\text{LUMO}) - 0.35\phi_{91} - 0.16\phi_{93} + \cdots$$

The C_2H_4 part:

$$\psi_1' = 0.12\psi_1 + 0.27\psi_2 + 0.28\psi_6(\text{HOMO}) - 0.91\psi_7(\text{LUMO}) - 0.11\psi_{12} + \cdots$$

$$\psi_2' = 0.15\psi_5 + 0.94\psi_6(\text{HOMO}) + 0.27\psi_7(\text{LUMO}) + \cdots$$

The PIO-1 of the catalyst part is composed mainly of the Mo $4d_{z2}$, Mo $4d_{xz}$ and C^1 $2p_z$ orbitals, whereas the PIO-1 of the C_2H_4 part consists mostly of the $2p_z$ orbital of C^3 and, to less extent, of the $2p_z$ orbital of C^2. The PIO-2 of the catalyst part is predominantly a mixture of the C^1 $2p_z$ and Mo $4d_{z2}$ orbitals. The $2p_z$ orbital of C^2 is the main component of the PIO-2 of the C_2H_4 part, while the contribution of the C^3 $2p_z$ orbital is much lower. The example LCAO representations of the PIO-1 and PIO-2 for **5ts** are given below.

The catalyst part:

$$\phi_1' = -0.10\text{Mo5s} - 0.53\text{Mo4d}_{z2} + 0.60\text{Mo4d}_{xz} + 0.11\text{C}^1\text{2s} + 0.45\text{C}^1\text{2p}_z + 0.16\text{O}^2\text{2p}_x + \cdots$$

$$\phi_2' = -0.18\text{Mo5s} - 0.26\text{Mo5p}_z - 0.64\text{Mo4d}_{z2} - 0.11\text{C}^1\text{2s} - 0.60\text{C}^1\text{2p}_z + 0.11\text{O}^2\text{2p}_y + 0.11\text{O}^3\text{2p}_z + 0.11\text{H}^1\text{1s} + 0.11\text{H}^2\text{1s} + \cdots$$

Table 7
The occupation numbers of the PIOs of the transition states

	PIO-1			PIO-2			PIO-3		
	Catalyst	C_2H_4	Total	Catalyst	C_2H_4	Total	Catalyst	C_2H_4	Total
1ts	1.42	0.90	2.32	0.75	1.32	2.07	1.34	1.85	3.19
2ts	1.40	0.84	2.24	0.65	1.43	2.08	0.94	1.87	2.81
3ts	1.44	0.83	2.27	0.66	1.41	2.07	1.11	1.88	2.99
4ts	1.42	0.89	2.31	0.73	1.32	2.05	1.28	1.85	3.13
5ts	1.46	0.82	2.28	0.65	1.42	2.07	1.11	1.87	2.98
6ts	1.51	0.74	2.25	0.54	1.54	2.08	0.78	1.91	2.69

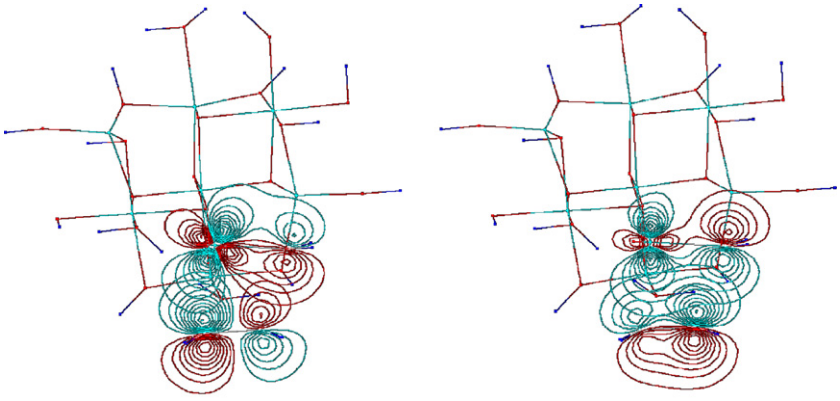

Fig. 4. Countur maps of the PIO-1 and PIO-2 of the transition state **5ts**.

The C_2H_4 part:

$$\psi_1' = -0.50C^2 2p_z - 0.15C^3 2s + 0.10C^3 2p_x + 0.88C^3 2p_z - 0.20H^3 1s - 0.21H^4 1s + 0.13H^5 1s + 0.12H^6 1s + \cdots$$

$$\psi_2' = 0.81C^2 2p_z + 0.17C^3 2p_x + 0.37C^3 2p_z + \cdots$$

On the contrary to the ethene complexes, the catalyst part of the PIO-1 is more occupied in the transition states than the C_2H_4 part and, consequently, the C_2H_4 part of the PIO-2 is more occupied than the catalyst part (Table 7). This is consistent with the analysis of the LCMO of the PIO-1 and PIO-2 and indicates that here the PIO-1 represents electron donation from the catalyst to the C_2H_4 moiety, while the PIO-2 represents donation from the C_2H_4 part to the catalyst. Compared to the ethene complexes, the order of the PIO-1 and PIO-2 of the transition states is reverse, which is also seen from Figs. 3 and 4.

The overlap populations of the PIO-1 and PIO-2 are positive and do not differ very much one from another (Table 8). The OPs are clearly higher than the corresponding values for the ethene complexes (Table 5), which shows more advanced electron delocalisation in the transition states. This is connected with the formation of two single bonds: Mo-C^3 and C^1–C^2, confirmed by the analysis of the LCAO representations of the PIOs as well as by the inspection of the contour maps in Fig. 4. Similarly as in the case of the ethene complexes, the PIO-3 orbital is antibonding (Tables 7 and 8).

The obtained results suggest that the Mo–C^3 and C^1–C^2 bonds are formed in an asynchronous manner, although both bonds are already developed in the transition state. However, the analysis of the PIO orbitals of the alkene complexes and the transition states indicates that the formation of the C^1–C^2 bond follows behind the Mo–C^3 bond formation. This is consistent with other reported results for similar systems [28,29], as well as with the previous DFT study of the molybdena-alumina catalysts [13,14].

3.3. Reactivity of the Mo methylidene centres

It was shown on the basis of the PIO analysis that total overlap population ($\sum$OP), indicating the strength of the interaction between two considered parts of the system, can be a reliable and convenient reactivity index [18,19,26]. In Table 9, the total overlap populations of the PIOs of the ethene complexes and

Table 8
The overlap populations of the PIOs of the transition states

	PIO-1	PIO-2	PIO-3
1ts	0.198	0.263	−0.062
2ts	0.270	0.345	−0.014
3ts	0.227	0.310	−0.023
4ts	0.204	0.268	−0.054
5ts	0.224	0.305	−0.043
6ts	0.245	0.331	−0.006

Table 9
The total overlap populations ($\sum$OP) and the relative energies of the structures studied (ΔE, kJ mol^{-1})

	$\sum$OP	ΔE
6et	0.282	−83
6et′	0.163	–
6ts	0.516	−82
2et	0.225	−34
2et′	0.145	–
2ts	0.521	−22
5et	0.204	−10
5et′	0.090	–
5ts	0.430	−4
3et	0.146	−4
3et′	0.081	–
3ts	0.463	6
4et	0.125	1
4et′	0.065	–
4ts	0.372	10
1et	0.093	–
1et′	0.044	–
1ts	0.352	51

transition states are listed together with their DFT energies, related to the energies of the reactants (Mo methylidene centre + ethene). These energetic parameters allow us to compare the reactivity of the Mo methylidene centres **1**–**6** towards ethene. Therefore, on the basis of the DFT calculations, the following reactivity order is predicted:

$$\mathbf{6} > \mathbf{2} > \mathbf{5} > \mathbf{3} > \mathbf{4} > \mathbf{1} \quad (7)$$

As can be seen from Table 9, the $\sum$OP for the ethene complexes **1et**–**6et** and **1et′**—**6et′** changes in the same decreasing sequence as (7). Thus, the $\sum$OP for the respective Mo alkene-alkylidene complexes can be a reactivity index applied in studies of molybdenum-based olefin metathesis catalysts. Moreover, the time-consuming geometry optimization of the alkene complexes, employing adequate, high-level theoretical methods, appears not to be necessary. The approximate geometry of the complexes (**1et′**–**6et′**, Table 1) is a sufficient approach to obtain satisfactory results (Table 9). In such a case, only the appropriate geometries of the Mo alkylidene complexes and the alkene molecule are needful.

When the transition states are concerned, the following sequence of the $\sum$OP can be read from Table 9:

$$\mathbf{2ts} \cong \mathbf{6ts} > \mathbf{3ts} > \mathbf{5ts} > \mathbf{4ts} > \mathbf{1ts} \quad (8)$$

This sequence differs from the reactivity order (7). It is seen that the order of **2ts** and **6ts**, as well as the order of **3ts** and **5ts** are reversed in (8), compared to (7). However, the differences between the $\sum$OP values for both pairs are not significant. Therefore, an approximate prediction of the activity of the Mo methylidene complexes towards alkene, based on the $\sum$OP for the transition states, is still possible.

4. Conclusions

The PIO analysis has been applied to study the first step of the catalytic cycle of ethene metathesis, i.e., ethene addition to Mo methylidene centres located on γ-alumina. The PIO approach has appeared to be a useful tool for both qualitative and quantitative description of the process.

It is concluded that at the early stage of the reaction, electron donation from the π orbital of ethene to the unoccupied d orbitals of the Mo methylidene site is more significant that the back-donation from the occupied space of the catalyst to the ethene π^* orbital. Along the reaction path leading to the molybdacyclobutane intermediate, the formation of the Mo–C_{ethene} bond is followed by the $C_{carbene}$–C_{ethene} bond formation.

The total overlap population between the Mo methylidene part and the C_2H_4 fragment of the Mo ethene-methylidene complex decreases with a decrease of the reactivity of the Mo methylidene centre towards ethene. Thus, the $\sum$OP is expected to be a useful reactivity index for the molybdenum-based olefin metathesis catalysts.

References

[1] K.J. Ivin, J.C. Mol, Olefin Metathesis and Metathesis Polymerization, Academic Press, London, 1997.
[2] J.C. Mol, J. Mol. Catal. A 213 (2004) 39.
[3] J.L.G. Fierro, J.C. Mol, in: J.L.G. Fierro (Ed.), Metal Oxides: Chemistry and Applications, Taylor & Francis, Boca Raton, 2006, p. 517.
[4] Y. Iwasawa, H. Kubo, H. Hamamura, J. Mol. Catal. 28 (1985) 191.
[5] A.N. Startsev, O.V. Klimov, E.A. Khomyakova, J. Catal. 139 (1993) 134.
[6] W. Yi, M. Schwidder, W. Grünert, Catal. Lett. 86 (2003) 113.
[7] J. Handzlik, J. Ogonowski, J. Stoch, M. Mikołajczyk, Appl. Catal. A 273 (2004) 99.
[8] J. Handzlik, J. Ogonowski, J. Stoch, M. Mikołajczyk, P. Michorczyk, Appl. Catal. A 312 (2006) 213.
[9] H. Aritani, O. Fukuda, T. Yamamoto, T. Tanaka, S. Imamura, Chem. Lett. (2000) 66.
[10] K.A. Vikulov, I.V. Elev, B.N. Shelimov, V.B. Kazansky, J. Mol. Catal. 55 (1989) 126.
[11] J.-L. Hérisson, Y. Chauvin, Makromol. Chem. 141 (1971) 161.
[12] J. Handzlik, J. Ogonowski, Catal. Lett. 88 (2003) 119.
[13] J. Handzlik, J. Ogonowski, R. Tokarz-Sobieraj, Catal. Today 101 (2005) 163.
[14] J. Handzlik, Surf. Sci. 601 (2007) 2054.
[15] H. Fujimoto, T. Yamasaki, H. Mizutani, N. Koga, J. Am. Chem. Soc. 107 (1985) 6157.
[16] H. Fujimoto, Acc. Chem. Res. 20 (1987) 448.
[17] N. Ichikawa, S. Sato, R. Takahashi, T. Sodesawa, J. Mol. Catal. A 231 (2005) 181.
[18] A. Shiga, M. Haruta, Appl. Catal. A 291 (2005) 6.
[19] A. Shiga, N. Katada, M. Niwa, Catal. Today 111 (2006) 333.
[20] M.J. Frisch, G.W. Trucks, H.B. Schlegel, G.E. Scuseria, M.A. Robb, J.R. Cheeseman, J.A. Montgomery Jr., T. Vreven, K.N. Kudin, J.C. Burant, J.M. Millam, S.S. Iyengar, J. Tomasi, V. Barone, B. Mennucci, M. Cossi, G. Scalmani, N. Rega, G.A. Petersson, H. Nakatsuji, M. Hada, M. Ehara, K. Toyota, R. Fukuda, J. Hasegawa, M. Ishida, T. Nakajima, Y. Honda, O. Kitao, H. Nakai, M. Klene, X. Li, J.E. Knox, H.P. Hratchian, J.B. Cross, V. Bakken, C. Adamo, J. Jaramillo, R. Gomperts, R.E. Stratmann, O. Yazyev, A.J. Austin, R. Cammi, C. Pomelli, J.W. Ochterski, P.Y. Ayala, K. Morokuma, G.A. Voth, P. Salvador, J.J. Dannenberg, V.G. Zakrzewski, S. Dapprich, A.D. Daniels, M.C. Strain, O. Farkas, D.K. Malick, A.D. Rabuck, K. Raghavachari, J.B. Foresman, J.V. Ortiz, Q. Cui, A.G. Baboul,

S. Clifford, J. Cioslowski, B.B. Stefanov, G. Liu, A. Liashenko, P. Piskorz, I. Komaromi, R.L. Martin, D.J. Fox, T. Keith, M.A. Al-Laham, C.Y. Peng, A. Nanayakkara, M. Challacombe, P.M.W. Gill, B. Johnson, W. Chen, M.W. Wong, C. Gonzalez, J.A. Pople, Gaussian 03, Revision C.02, Gaussian Inc., Wallingford, CT, 2004.
[21] A.D. Becke, J. Chem. Phys. 98 (1993) 5648.
[22] P.J. Stevens, J.F. Devlin, C.F. Chabalowski, M.J. Frisch, J. Phys. Chem. 98 (1994) 11623.
[23] P.J. Hay, W.R. Wadt, J. Chem. Phys. 82 (1985) 299.
[24] T.H. Dunning Jr., P.J. Hay, in: H.F. Schaefer III (Ed.), Modern Theoretical Chemistry, vol. 3, Plenum, New York, 1976, p. 1.
[25] H. Katsumi, Y. Kikuzono, M. Yoshida, A. Shiga, H. Fujimoto, LUMMOX, Sumitomo Chemical Co., Ltd., Tokyo, 1999.
[26] T. Motoki, A. Shiga, J. Comput. Chem. 25 (2004) 106.
[27] E. Folga, T. Ziegler, Organometallics 12 (1993) 325.
[28] Y.-D. Wu, Z.-H. Peng, J. Am. Chem. Soc. 119 (1997) 8043.
[29] T.P.M. Goumans, A.W. Ehlers, K. Lammertsma, Organometallics 24 (2005) 3200.